J Mater Sci (2012) 47:503–507
DOI 10.1007/s10853-011-5826-8

Hexagonal nickel oxide nanoplate-based electrochemical supercapacitor

Zhihong Zhu · Jing Ping · Xiaopeng Huang · Jiugang Hu · Qiyuan Chen · Xiaobo Ji · Craig E. Banks

Received: 4 June 2011 / Accepted: 26 July 2011 / Published online: 13 August 2011

Abstract A facile approach is demonstrated for the preparation of hexagonal NiO porous nanoplates via surfactant self-assembly. These NiO nanoplates are produced via a singe-step process via thermal decomposition at high temperatures using a nickel salt and the surfactant cetyltrimethylammonium bromide. The NiO nanostructures are hexagonal in shape with diameters of 300 nm and thickness of 20 nm. The NiO nanoplates are found to exhibit a beneficial specific capacitive performance of 286.7 F g^{-1}.

Introduction

Supercapacitors, also termed electrochemical capacitors (EC) are electronic components that can be rapidly charged and discharged and relied upon storing energy reliably for long periods [1–3]. Supercapacitors are widely used in pulse applications to reduce the load on the battery allowing a longer battery working life, providing a solution to the mismatch between the fast growth in power required by devices and the inability of batteries to efficiently discharge at high rates [4, 5].

The materials mostly used as electrochemical double layer capacitors (EDLC) are based on carbonaceous materials such as activated carbon [6, 7], carbide-derived carbon [8, 9], graphene [10–12], and carbon nanotubes [13–16] which have a large surface area for the charge to reside. Supercapacitors in the other class, called pseudo-capacitors, utilize transition metal oxides, or electrically conducting polymers as electrode materials [1]. The storage mechanism in this case is based upon fast surface faradaic reactions while the amount of charge held is proportional to the voltage [1]. While supercapacitors benefit from the highest known power capability (10 kW kg^{-1}), high current capability, ease of maintenance, and almost unlimited cycle life (>10^6 cycles) [1, 4], their specific capacitances for the applications in the next generation all-electric cars and cars based on fuel cells that use hydrogen or alcohol as clean and renewable energy media are still far away to meet the performances and cost requirements, in particular providing power boosts to start the engine or to assist acceleration.

In order for supercapacitors to become commercially viable and extensively used, the energy that they can store needs to significantly increase and to achieve supercapacitors with sufficient energy for higher requirements remains a challenge. Extensive efforts have been devoted to improve the specific capacitance of supercapacitors by introducing pseudo-capacitive metal oxides. Compared with the EDLC-based capacitors, pseudo-capacitors based on transition metal oxide electrodes such as RuO_2, [17, 18] MnO_2, [19, 20] Co_3O_4, [21], and NiO [22–27] has attracted much attention because they can produce higher

Z. Zhu · J. Ping · X. Huang
Institute of Nano-Science and Technology Center, Huazhong Normal University, Wuhan 430079, People's Republic of China

J. Hu · Q. Chen · X. Ji (✉) · C. E. Banks (✉)
Institute of Metallurgical Physicochemistry, College of Chemistry and Chemical Engineering, Central South University, Changsha 410083, China
e-mail: xji.csu.edu@gmail.com

C. E. Banks
e-mail: c.banks@mmu.ac.uk

C. E. Banks
School of Chemistry and the Environment, Division of Chemistry and Environmental Science, Manchester Metropolitan University, John Dalton Building, Chester St, Manchester M1 5GD, UK

capacitances than double-layer carbonaceous materials. Impressively, nickel oxide is very attractive in view of its outstanding pseudo-capacitive behavior, practical availability, environmental compatibility, and lower cost when compared to the state-of-the-art supercapacitor material RuO_2. Despite its importance, efforts are still needed to further improve the practical use of nickel oxide supercapacitors.

A key methodology to boost the specific capacitance of such nickel-based materials is their morphological and/or chemical composition design at the nanometer-scale, because high surface-to-volume ratio with suitable pore sizes is desirable for the penetration of electrolytes and reactants into the whole electrode matrix, and can promote the electric double-layer capacitances and accommodate a large amount of superficial electroactive species to participate in faradaic redox reactions. Thus, hexagonal NiO nanoplates are being synthesized and tested in the presence of an alkaline electrolytic solution.

In this study, we report a novel, template-free approach to fabricate a hexagonal symmetry structure of NiO porous nano-plates. We demonstrate that the unique structure of the nano-composite can accommodate the electroactive species accessible to fast faradaic reactions in bulk electrode materials, which shows better rate capability and great potential as electrode materials for supercapacitors. It is noted that the mesoporous NiO nano-plates were produced via a single-step process, by thermal decomposition of the as-synthesized $Ni(OH)_2$ plates at high temperature.

Experimental section

Materials and synthesis

All the chemicals were of analytical grade and used with out any further purification. $NiCl_2{\cdot}6H_2O$, ammonia (26%), and cetyltrimethylammonium bromide were purchased from Shanghai Chemical Co. LTD, China. All the experiments were carried out at 298 ± 3 K.

In a typical experiment, 4 mM of $NiCl_2{\cdot}6H_2O$ and 8 mM of ammonia (26%) as well as 2 mM of cetyltrimethylammonium bromide were dissolved in 40 mL of deionized water and stirred for 2 h at room temperature. Then the as-prepared solution was sealed into a Teflon-lined autoclave, followed by hydrothermal treatment at 160 °C for 24 h in an electric oven. After the treatment, greenish $Ni(OH)_2$ products were collected by filtration, washed three times with deionized water, and dried for 10 h at 80 °C (yield: 49%). NiO nano-plates could be obtained by thermal decomposition of the as-synthesized $Ni(OH)_2$ powder at 300 °C for 3 h in air.

Characterization of NiO nanoplates

The morphologies of the catalyst were characterized by transmission electron microscopy (TEM) (Japan JEOL JEM-200CX, transition electron microscope). High-resolution TEM (HRTEM) images were obtained on a Philips TECNAI F-30 FEG instrument at an accelerating voltage of 300 kV. SEM images and the energy dispersive spectrum (EDS) were obtained by a JEOL S-4800 apparatus. The phase purity of the products were characterized by X-ray power diffraction (XRD), (Shimadzu XD-3A X-ray diffractometer with Cu Kα radiation, $\lambda = 0.15417$ nm). The BET (Brunauer–Emmett–Teller) surface area was measured by ASAP2020 (Micromeritics, United States).

Electrochemical measurements

The working electrodes were prepared as following: 90 wt% of NiO powder was mixed with 5 wt% of acetylene black (499.9%) in an agate mortar until a homogeneous black powder was obtained. To this mixture, 5 wt% of poly(tetrafluoroethylene) was added with a few drops of ethanol. After briefly allowing the solvent to evaporate, the resulting paste was pressed at 12 MPa onto a nickel gauze. The electrode assembly was dried for 12 h at 80 °C in air. Each electrode had a geometric surface area of ~ 0.75 cm^2. Electrochemical measurements were carried out in 6 M aqueous KOH in a half-cell setup configuration at room temperature using CHI 660D electrochemical workstation (Shanghai Chenhua Instrument Co. Ltd., China). A platinum electrode and Hg–HgO electrode served as the counter electrode and the reference electrode, respectively. The specific capacity of the NiO is calculated via the following equation:

$$C = \frac{C}{m} = \frac{I \times \Delta t}{\Delta V \times m}$$

where I is the discharge current, m is the mass of the active materials (V is the potential drop during discharging (t is the total discharge time, and C is the specific capacity.

Results and discussion

The resulted mesoporous structure of these nanoplates can be verified by morphological analyses. Figure 1a reveals that NiO sheets are hexagonal tablets with diameters of 300 nm and thickness of 20 nm. Note that the hexagon side length of the nano-NiO (Fig. 1b) is around 200–250 nm. Figure 1c is the representative HRTEM images of as-synthesized nanoplates. It can be clearly seen from Fig. 1c that the NiO sheets have merits of mesoporous structures, interestingly, the pore size distribution calculated from

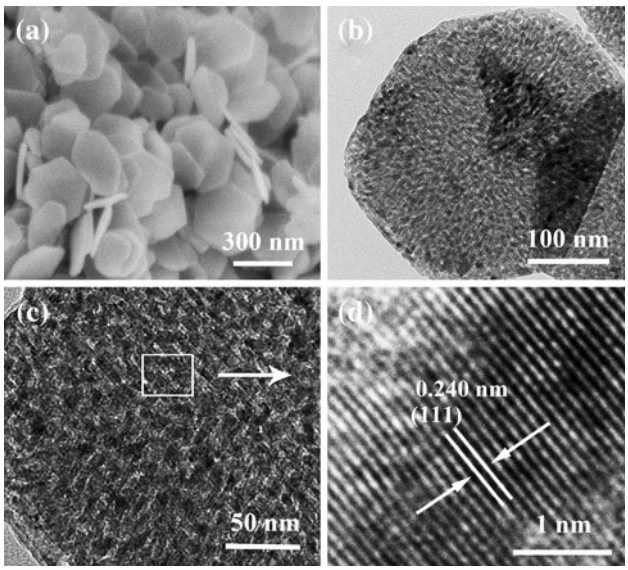

Fig. 1 SEM (**a**), TEM (**b**), and HRTEM (**c**, **d**) images of hexagonal mesoporous NiO nanoplates before milling in agate-mortar

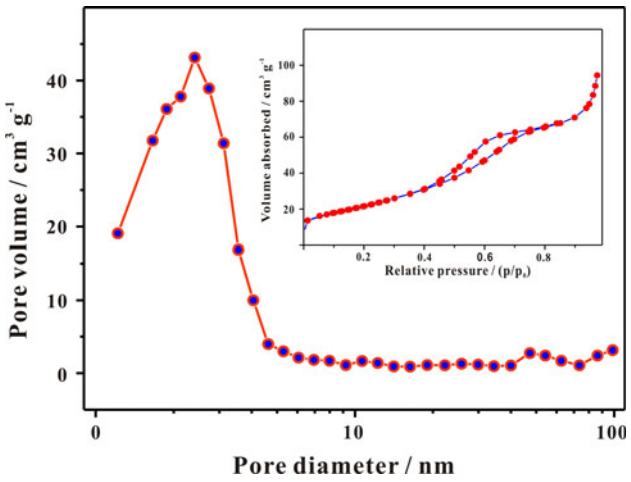

Fig. 2 A histogram of Barrett–Joyner–Halenda pore size distribution plot. The *inset* is the N_2 adsorption–desorption isotherm loop of NiO

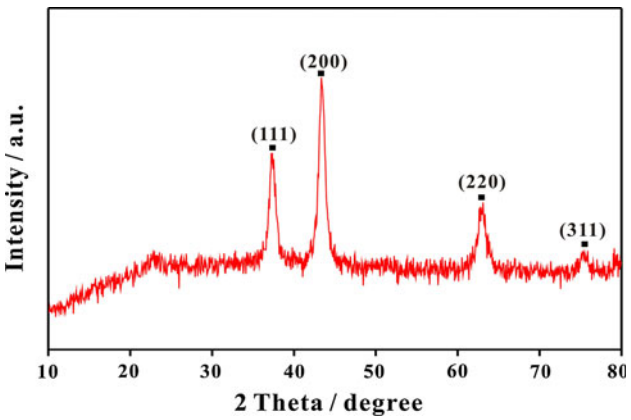

Fig. 3 XRD of hexagonal NiO nanoplates

Barrett–Joyner–Halenda (BJH) in Fig. 2 using the adsorption curve in the context of the BJH methodology further reveals the presence of hierarchical porosity. The textural properties of the NiO nanoplates are quantitatively shown as following: the specific surface area of the sample is 95 $m^2\ g^{-1}$ and a narrow pore-size distribution can be clearly observed with peak size at ca. 2.41 nm, such porosity would create many more convenient channels for electrolyte ions to transport and electrochemically access even more electroactive sites for energy storage as fast as possible at large current densities. Also via the N_2 adsorption–desorption isotherm of the synthesized NiO nano superstructure, the narrow hysteresis loop at a low relative pressure in Fig. 2 indicates that the porous structure is quite open and there is no significant delay in the capillary evaporation with respect to the capillary condensation of nitrogen. Remarkably, the lattice space observed from HRTEM images in Fig. 1d, 0.24 nm, is consistent with the XRD observations in Fig. 3. The well-defined peaks are centered around 2θ values of ca. 37, 43, 62, and 79°, corresponding to the (111), (200), (220), and (311) reflections, respectively.

Based on the above discussions, we summarize a proposed mechanism in Scheme 1. The layered unit possesses hexagonal symmetry (C6-type), in hydrotalcite-like compounds, where each Ni^{2+} is octahedrally bound to six hydroxyl groups and self-assemble to forming the octahedron of $Ni(OH)_2$. The octahedrons share their edges to form two dimensionally infinite brucite-like sheets, which then stack upon one another to form a nanoplate [28, 29]. In the process of heat treatment the hydrogen bonds associated with the two adjacent layers of hydroxyl ions were partially broken, releasing some water molecules and forming the molecule-sized pores resulted from decomposition of its precursor $Ni(OH)_2$. As a result, nanoparticles and mesopores coexist within the nanoplate. The mesopores could provide abundant surface areas, confirmed in BET test.

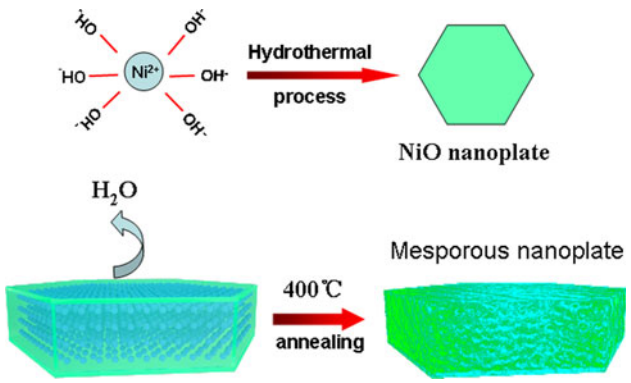

Scheme 1 The proposed NiO nanoplates mechanism

Cyclic voltammetric measurement (CV) was considered to be a suitable tool for estimating the difference between the non-Faradaic and Faradaic reactions. The CV response of the as prepared NiO electrode in 6 M aqueous KOH with a half-cell setup configuration is shown in Fig. 4a where a single oxidation wave at ca. +0.33 V (vs. Hg/HgO) and a corresponding reductive wave at ca. +0.19 V (vs. Hg/HgO) were observed, which is attributed to a quasi-reversible redox processes during the potential sweep of the NiO electrode, as following:

$$NiO + OH^- \underset{\text{discharge}}{\overset{\text{charge}}{\rightleftharpoons}} NiOOH + e^-$$

It is clear that the CV profiles exhibit pseudo-capacitance characteristics, very distinct from that of electric double-layer capacitance in which the shape is normally close to a nearly symmetrical rectangular shape. Note that with the increased scan rates the difference between the anodic and cathodic peak potential was increased, resulting in lower capacitance, which is in agreement with the result of chronopotentiometry measurements.

The applicability of supercapacitors can be directly evaluated by means of the galvanostatic charge–discharge method. Plots of voltage versus time for the NiO supercapacitors at various rates are presented in Fig. 4b. As expected, the nonlinear discharge curves were observed, and the corresponding specific capacitance was calculated using the formula provided in experimental section. Impressively, specific capacitances of NiO nanoplates calculated at 1, 2, 3, 5, and 10 A g^{-1} from the discharge curves is 286.7, 263.3, 253.6, 235.7, and 193.6 F g^{-1}, respectively, as shown in Fig. 4c. About 82.3% specific capacitance was retained even with the current density increasing from 1 to 5 A g^{-1}, and 67.6% capacitance left is still reasonable with 10 A g^{-1}. Owing to the porous surface of NiO plates, as shown in Fig. 2c, giving the well-connected 3D networked structures, the charge can store in these few nanometers pores more efficiently with a decreased particle size, which in turn increases active material usage. It should be noted that such rich porous structures can significantly reduce the OH^- ions diffusion lengths for the electrolyte ions and insure enough electrolyte ions to rapidly contact the much larger surfaces of the electroactive NiO nanoplates, leading to sufficient faradaic reactions at high current densities. Consistently excellent rate capability of NiO nanoplates over a wide range of current densities makes this nano-pore material particularly promising as supercapacitor electrodes.

In order to evaluate the electrochemical capacitance of the NiO samples as a function of the cyclability,

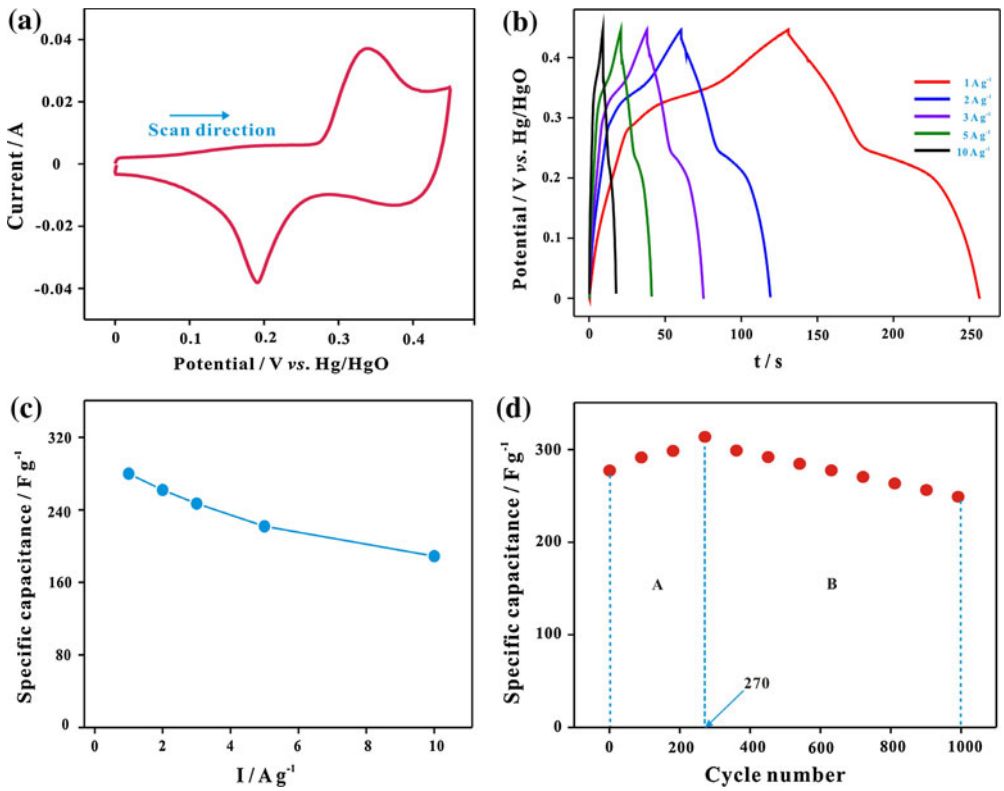

Fig. 4 CV curves at scan rate 10 mV s^{-1} in 6 M KOH (**a**), CP plots (**b**), and specific capacitance as a function of the current density (**c**), and cycle number (**d**) of the NiO nanoplates electrodes

continuous charge–discharge measurements over 1000 cycles at a current density of 1 A g^{-1} within a voltage range between 0.0 and 0.45 V in 6 M KOH electrolyte were conducted on NiO nanoplates samples, as shown in Fig. 4d. It is worth mentioning that the specific capacitances observed, instead of decreasing as in most cycle stability tests, was increased from ca. 286 to 310 F g^{-1} after 270 cycles, approximately 8.3%. Clearly those additional 270 cycles were needed to fully activate NiO material. Then it slightly decreases to 253 F g^{-1} after the subsequent 730 continuous cycles, remaining 88.5% of the original capacitances, which is considered insignificant. The great stability of 1000 continuous charge discharge cycles demonstrates that the galvanostatic charge–discharge processes do not induce significant micro-structural changes of the nano-plates NiO electrode materials as expected for pseudo-capacitance reactions. This specific capacitence is comparable to other unique structures reported in the literature such as urchin-like NiO nanostructures [27], Pine-cone structures, [26], NiO nanowall arrays [25]. Interestingly the specific capacitance of the NiO nanoplates are superior over MnO_2 nanoparticles [30] suggesting a larger surface area of the former over the latter. Note that of course RuO_2 has a higher specific capacitance but is unfortunately cost-prohibitive and hence why new capacitor materials are sought [31].

Conclusions

In conclusion, hexagonal nickel oxide nanoplates, a low-cost material of highly porosity, as well as electrochemical activity was successfully prepared with a simple self-assembly process. The unique structures of nickel oxide nanoplates can provide favorable paths for electrolyte penetration and transportation, achieving an relatively high specific capacitance of 310 F g^{-1} after a 270-cycle activation. The decay in the specific capacitance, based on this maximum value after a 1000-cycle test, was insignificant, revealing the excellent stability of the product. This study demonstrates the design of a next-generation supercapacitor material by successfully preparing a low-cost, high-performance oxide with a cost-effective preparation process, and the strategy reported here can be viable to extend to the preparation of other transition metal oxides systems.

Acknowledgements Financial supports from the National Natural Science Foundation of China (No. 21050110115), International Joint Project from The Royal Society (No. JP090644), Hunan Province Foundation of Natural Science (10JJ6026), and China Postdoctoral Science Foundation funded project (20100471226) are greatly appreciated.

References

1. Conway BE (1999) Electrochemical supercapacitors. Kluwer Academic/Plenum Press, New York
2. Conway BEJ (1991) Electrochem Soc 138:1539
3. Winter M, Brodd RJ (2004) Chem Rev 104:4245
4. Simon P, Gogotsi Y (2008) Nat Mater 7:845
5. Miller JR, Simon P (2008) Science 321:651
6. Largeot C, Portet C, Chmiola J, Taberna PL, Gogotsi Y, Simon PJ (2008) Am Chem Soc 130:2730
7. Raymundo-Pinero E, Leroux F, Beguin F (2006) Adv Mater 18:1877
8. Gogotsi Y, Nikitin A, Ye H, Zhou W, Fischer JE, Yi B, Foley HC, Barsoum MW (2003) Nat Mater 2:591
9. Chmiola J, Largeot C, Taberna PL, Simon P, Gogotsi Y (2010) Science 238:480
10. Chen S, Zhu J, Wang X (2010) ACS Nano 4:6212
11. Wang HL, Casalongue HS, Liang YY, Dai HJJ (2010) Am Chem Soc 132:7472
12. Miller JR, Outlaw RA, Holloway BC (2010) Science 329:1637
13. Lee SW, Kim BS, Chen S, Shao-Horn Y, Hammond PTJ (2009) Am Chem Soc 131:671
14. Chen PC, Shen G, Shi Y, Chen HT, Zhou CW (2010) ACS Nano 4:4403
15. Yu CJ, Masarapu C, Rong JP, Wei BQ, Jiang HQ (2009) Adv Mater 21:4793
16. Futaba DN, Hata K, Yamada T, Hiraoka T, Hayamizu Y, Kakudate Y, Tanaike O, Hatori H, Yumura M, Iijima S (2006) Nat Mater 5:987
17. Hu CC, Chang KH, Lin MC, Wu YT (2006) Nano Lett 6:2690
18. Sugimoto W, Iwata H, Yasunaga Y, Murakami Y, Takasu Y (2003) Angew Chem 42:4092
19. Liu HJ, Jin LH, He P, Wang CX, Xia YY (2009) Chem Comm 44:6813
20. Reddy LM, Shaijumon MM, Gowda SR, Ajayan PMJ (2010) Phys Chem C 114:658
21. Wei TY, Chen CC, Chien HC, Lu SY, Hu CC (2010) Adv Mater 22:347
22. Prasad KR, Miura N (2004) Appl Phys Lett 85:4199
23. Kim JH, Zhu K, Yan YF, Perkins CL, Frank AJ (2010) Nano Lett 10:4099
24. Hu GX, Tang CH, Li CX, Li HM, Wang Y, Gong H (2011) J Electrochem Soc 158:A695
25. Zhu JH, Jiang JA, Liu JP, Ding RM, Ding H, Feng YM, Wei GM, Huang XT (2011) J Solid State Chem 184:578
26. Meher SK, Justin P, Rao GR (2010) Electrochem Acta 55:8388
27. Liu XM, Zhang XG, Fu SY (2006) Mat Res Bull 41:620
28. Sato H, Yamagishi A, Kawamura KJ (2001) Phys Chem B 105:7990
29. Qi Y, Qi HY, Li JH, Lu CJJ (2008) Crys Growth 310:4221
30. Wang HQ, Yang GF, Li QY, Zhong XX, Wang FP, Li ZS, Li YH (2001) New J Chem 35:469
31. Hyun T-S, Tuller HL, Youn D-Y, Kim H-G, Kim I-D (2010) J Mat Chem 20:9172